Hindawi
Geofluids
Volume 2022, Article ID 1057653, 13 pages
https://doi.org/10.1155/2022/1057653

WILEY | Hindawi

Research Article

Investigation of Multiscaled Pore Structure of Gas Shales using Nitrogen Adsorption and FE-SEM Imaging Experiments

Aiwei Zheng,[1] Hanyong Bao,[1] Li Liu,[1] Mingkai Tu,[2] Changpeng Hu,[3] and Lei Yang[4]

[1]*Research Institute of Exploration and Development, Jianghan Oilfield Branch Company, SINOPEC, Wuhan 430223, China*
[2]*Key Laboratory of Tectonics and Petroleum Resources (China University of Geosciences), Ministry of Education, Wuhan 430074, China*
[3]*China Petroleum Technology and Development Corporation, Beijing 100009, China*
[4]*Tianjin Gangrui Petroleum Engineering Technology Company Limited, Tianjin 300280, China*

Correspondence should be addressed to Mingkai Tu; tmk0214@cug.edu.cn

Received 3 September 2021; Revised 8 December 2021; Accepted 20 May 2022; Published 7 June 2022

Academic Editor: Mohammed Fattah

Nanopore in shales is the place for hydrocarbon accumulation and migration. However, there is a lack of understanding of the nanopore structure with regard to their ultratight and multiscaled nature. Here, the porous morphology of gas shales from the Sichuan Basin of China was investigated using field emission-scanning electronic microscopy (FE-SEM) with high resolution. Low-pressure nitrogen adsorption experiments at 77 K were conducted to obtain the adsorption-desorption isotherms, BET-specific surface area, pore size distribution, pore volume, and average pore diameter values. Research results show that pores of the studied shales are at the nanometer scale, and the average pore diameter is between 3 and 5 nm. The pore structure of these shales is complicated, which is not only predominately mesopores (pore diameter at 2–50 nm) but also some micropores (pore diameter < 2 nm) and macropores (pore diameter > 50 nm). The specific surface area of shales ranges from 13 to 30 m^2/g. The micropore volume and mesopore volume occupy the total pore volume highly up to 77%–92%, which indicates that micropores and mesopores are the main storage place for shale gas. Through the analysis of adsorption isotherms and hysteretic loops, there are mainly two kinds of pores in shales, including ink-bottle-like pores and slit pores. Micropores of these shales are mainly related to organic matter, while macropores are mainly related to clay minerals. The estimation about porosity using the combined physical model shows that organic matter and clay minerals contribute about 50% and 33% to the porosity of these shales, respectively.

1. Introduction

Conventional reservoirs mainly refer to the sandstone reservoir and carbonate reservoir, whose pore diameter is always beyond 1 μm [1–3]. However, with the development and exploration of unconventional reservoirs, shales have received lots of interest because of their emergence as hydrocarbon reservoirs. Pore structure of shales is a fundamental question during shale development. As a kind of supertight hydrocarbon reservoir, the pore dimension of shales is commonly far below the that of sandstone or carbonate reservoirs, and the pores are mainly nanometer in scale [4–6]. Pore diameter of shales in the Fort Worth Basin is 5–750 nm with an average pore diameter of 100 nm. The pore diameter of shallow shales in the Beaufort-MacKenzie Basin is 25–10 μm while that of deep shales is 2.5–25 nm [7–9]. The pore diameter of shales in North America is 5–160 nm, mainly 8–100 nm, while the pore diameter of maturated shales in the Sichuan Basin is about 100 nm [10–12]. Pore structure characteristics have a great effect on gas storage, adsorption capacity, and gas migration in the nanospace [13–16].

The methodology used for the reservoir structure of conventional reservoirs mainly includes thin section analysis, mercury injection, and scanning electronic microscopy (SEM). However, plenty of pores in shales cannot be clearly observed by conventional analysis methods because of their nanoscaled characteristics. The thin section analysis is

commonly applied in conventional reservoirs. Mercury injection is mainly performed on connected mesopores and macropores. The optical microscope and SEM cannot effectively detect pores at the nanometer scale in shales because of their low resolution.

In this study, field emission scanning electronic microscopy (FE-SEM) with high revolution is applied to observe the morphology of the nanopore structure of shales. Nitrogen adsorption experiments at low temperature are conducted to obtain the adsorption-desorption isotherms. Then, the chemical theory is used to analyze the adsorption-desorption isotherms, and quantitative pore structure parameters are obtained, such as specific surface area, pore size distribution, pore volume, and average pore diameter. The Horvath-Kawazoe (H-K) model is used to calculate the adsorption isotherm at the low relative pressure range. What is more, the relation between types of hysteresis loop and the pore structure characterization are analyzed in detail according to adsorption and condensation theory.

2. Samples and Experiments

2.1. Samples. Marine shale samples were collected from a shale gas well drilled in the Jiaoshiba area of Sichuan Basin, China. The Jiaoshiba area is the largest shale gas production area in China. The accumulated amount of produced shale gas was more than 300×10^8 m^3, though it was only developed since 2013. Shale gas resources in the Jiaoshiba area are mainly concentrated in the southern Paleozoic marine shales with strong structural transformation, complex ground stress, and deep burial [17, 18]. The Jiaoshiba tectonically located in the eastern Sichuan block fold in the eastern Sichuan Basin, and the west of the Qiyueshan fault [17]. The Jiaoshiba structure is a narrow and steep anticline in the N/E direction or nearly N/S direction. The structural deformation in the main body of the Jiaoshiba area is relatively weak. It shows a box-like fault anticline; that is, the top of the Jiaoshiba anticline is wide and slow, while the dip angle of the stratum is small. Faults do not develop in the main body of the Jiaoshiba area but develop in the two wings of the anticline structure [19].

Shale samples were collected and subjected to the total organic carbon (TOC) test and X-ray diffraction (XRD) experiment. The tested TOC content of the samples is between 1.0% and 5.4%, with an average value of 2.5%. Minerals in the samples contain quartz, orthoclase, plagioclase, carbonates, and clay minerals (Table 1). Quartz and clays are the main minerals in these samples. Quartz in the investigated sample is from 26% to 60%, with an average value of 37.2%. Total clay minerals vary from 25% to 59% and averages 41.7%.

2.2. Experiments. Low pressure nitrogen adsorption experiment is conducted on the QUADRASORB SI surface and porosity analyzer, which uses a static volumetric method to measure the amount of adsorbed gas. This instrument can measure the nanopores ranging from 0.35 nm to 400 nm in diameter. The minimum detectable specific surface area is 0.0005 m^2/g, and the minimum detectable pore volume is 0.0001 cm^3/g. Before nitrogen adsorption experiments, all the shale samples were degassed at 105°C for more than 8 hours under a vacuum of 10 μm Hg, which ensures removal of any bound and capillary water adsorbed with the clays [11]. Reagent-grade nitrogen (99.999%) is used for adsorbent at 77.35 K.

FEI field emission scanning electronic microscopy (FE-SEM) was used to observe the microscope morphology and pore structure of selected shales. FE-SEM provides "as received" images on pore structure with the highest resolution of 1.2 nm and the largest magnification of 25-200k. The tests are preceded on a high vacuum environment.

Helium pycnometry was utilized to measure the porosity of shale samples. Cylinder samples were dried at 105°C more than 8 hours until the weight is stable. Then, the bulk density of the cylinder samples was determined by using a caliper and the dry weight. After that, the cylinder was put into a helium pycnometer to measure the skeletal density. These values were achieved by multiple helium expansions from the reference cell to the sample cell. Then, porosity of the shale samples is calculated according to the bulk density and skeletal density values.

3. Results and Discussion

3.1. Porosity. Porosity of the studied shales ranges from 1.8% to 4.8%with an average of 3.4% (Table 2). Porosity of these shales increases with increasing TOC content. Shale samples rich in organic matter have relatively high porosity.

3.2. Nitrogen Adsorption-Desorption Isotherms. Figure 1 shows the nitrogen adsorption-desorption isotherms of the representative shale samples collected from the Jiaoshiba area. Qualitative assessment of the porous structure can be obtained based on the isotherms. Although there is difference in the adsorbed amount of nitrogen, the isotherms are all like a reverse "S" in shape. The isotherms of shales belong to type IV according to the International Union of Pure and Applied Chemistry (IUPAC) classification [20]. This indicates that the adsorption mechanism transforms from the monomolecular layer adsorption to the multilayer adsorption because there is no restriction of adsorption space on the surface of the adsorbent. The adsorption isotherm rises slowly in low relative pressure and then bulges, while the slop of the isotherms declines. When the relative pressure increases to a special turning point, the isotherm nearly becomes a straight line, and the slop becomes a constant. These indicate the completion of monomolecular layer adsorption and the outset of multilayer adsorption. The adsorbance at the turning point is approximately equal to the monolayer capacity [21]. After the linear stage, the isotherm goes up sharply with the increasing relative pressure. When the equilibrium pressure approaches the saturated vapor pressure of nitrogen, the adsorbed amount of nitrogen still does not reach saturation, and the capillary condensate of nitrogen commences at the surface of shales. The detection of the type IV adsorption isotherm means that multilayer adsorption has happened on the surface of the

Table 1: TOC and mineral compositions of the investigated marine shale samples.

Sample	Basin	Stratigraphy	TOC content (wt%)	Quartz (wt%)	Orthoclase (wt%)	Plagioclase (wt%)	Carbonates (wt%)	Total clays (wt%)
JY41	Sichuan	S1l	1.00	34.70	1.10	3.60	5.90	53.00
JY51	Sichuan	S_1l	1.23	26.80	0.80	5.80	4.40	58.90
JY55	Sichuan	S_1l	1.38	29.80	0.90	5.10	5.20	56.50
JY61	Sichuan	S_1l	1.58	27.20	0.70	5.50	10.00	53.60
JY71	Sichuan	S_1l	1.02	26.00	1.10	7.30	27.00	35.80
JY85	Sichuan	S_1l	2.11	28.20	1.40	6.80	12.50	47.20
JY91	Sichuan	S_1l	2.60	38.00	1.10	4.80	7.70	45.90
JY101	Sichuan	S_1l	2.15	38.10	1.20	3.30	13.10	38.60
JY105	Sichuan	S_1l	2.78	43.10	1.10	5.50	13.10	32.50
JY111	Sichuan	S_1l	3.29	45.50	1.20	4.20	10.60	32.20
JY115	Sichuan	S_1l	3.76	31.30	1.60	6.20	23.00	33.50
JY119	Sichuan	S_1l	5.36	55.30	1.50	4.40	7.60	28.70
JY121	Sichuan	S_1l	3.65	59.50	1.20	2.20	7.90	25.40

Table 2: Pore structure parameters of the investigated marine shale samples.

Sample	Helium porosity (%)	Surface area (m^2/g)	Total pore volume (cm^3/g)	Pore diameter (nm)	Micropore volume percentage (%)	Mesopore volume percentage (%)	Macropore volume percentage (%)
JY41	1.81	2.79	0.0179	5.16	29.02	48.38	22.60
JY51	2.19	13.88	0.0190	4.83	30.87	50.66	18.47
JY55	3.90	15.68	0.0214	5.03	29.78	48.99	21.22
JY61	4.10	17.00	0.0214	4.52	33.18	49.35	17.48
JY71	4.49	18.96	0.0162	4.86	30.81	46.58	22.61
JY85	4.00	13.36	0.0229	4.75	31.48	47.18	21.34
JY91	3.90	19.26	0.0225	4.42	33.87	48.98	17.16
JY101	3.30	20.36	0.0210	4.47	33.65	46.41	19.94
JY105	2.90	18.82	0.0217	4.57	32.86	46.02	21.12
JY111	2.70	19.04	0.0203	3.95	38.08	46.06	15.86
JY115	4.80	20.56	0.0244	3.84	37.50	44.43	18.07
JY119	4.80	25.44	0.0273	3.67	40.88	51.23	7.89
JY121	3.64	29.71	0.0216	4.16	35.97	54.05	9.99

adsorbent, whose pore dimension ranges from as small as a molecular size to being relatively infinite.

3.3. Assessment of Mesopores. The Brunauer-Emmett-Teller- (BET-) specific surface area is determined by applying the BET theory (equation (1)) to the gas adsorption data in the relative pressure ranging from 0.05 to 0.30 [22]:

$$\frac{P/P_0}{V(1-P/P_0)} = \frac{1}{V_m C} + \frac{C-1}{V_m C} \bullet \frac{P}{P_0}. \quad (1)$$

According the BET theory, $(P/P_0)/V(1-P/P_0)$ versus P/P_0 yields a straight line in the BET plot (Figure 2), and the BET monolayer capacity V_m and BET constant C can be derived from the slop and intercept of the linear line.

The BET-specific surface area can be calculated from the following equation using the monolayer capacity (equation (2)):

$$S = \frac{V_m N a_m}{22400} \times 10^{-18}. \quad (2)$$

Pore size distribution is determined from adsorption isotherms using the Barrett-Joyner-Halenda (BJH) method [23]. The BJH method is based on the Kelvin equation and Halsey equation and behaves better in describing pore size distribution of mesoporous material. The Kelvin equation provides the relationship between the pore radius and vapor pressure. It is assumed that all the pores of the solid adsorbent are rigid and cylindrical in shape, which functions as capillary tubes in adsorption and condensation

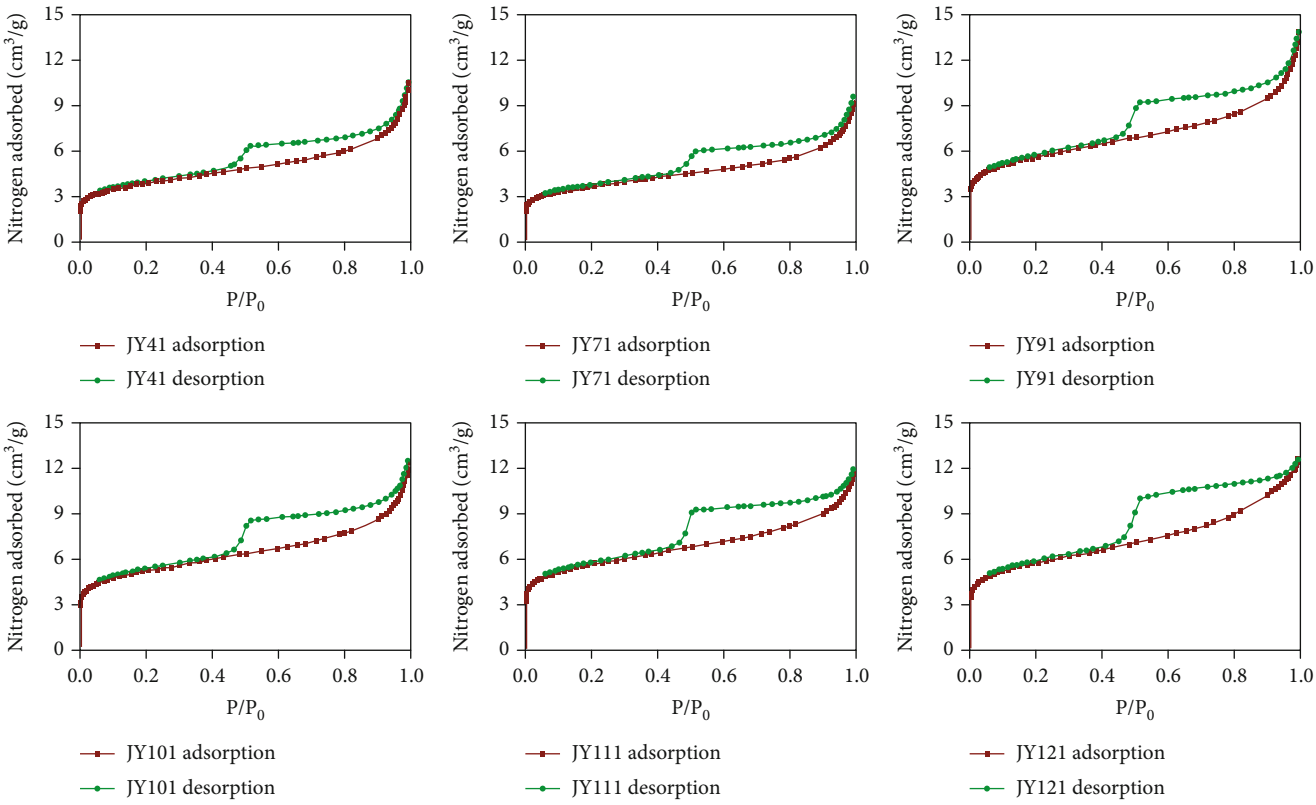

Figure 1: The nitrogen adsorption-desorption isotherms of the studied gas shales.

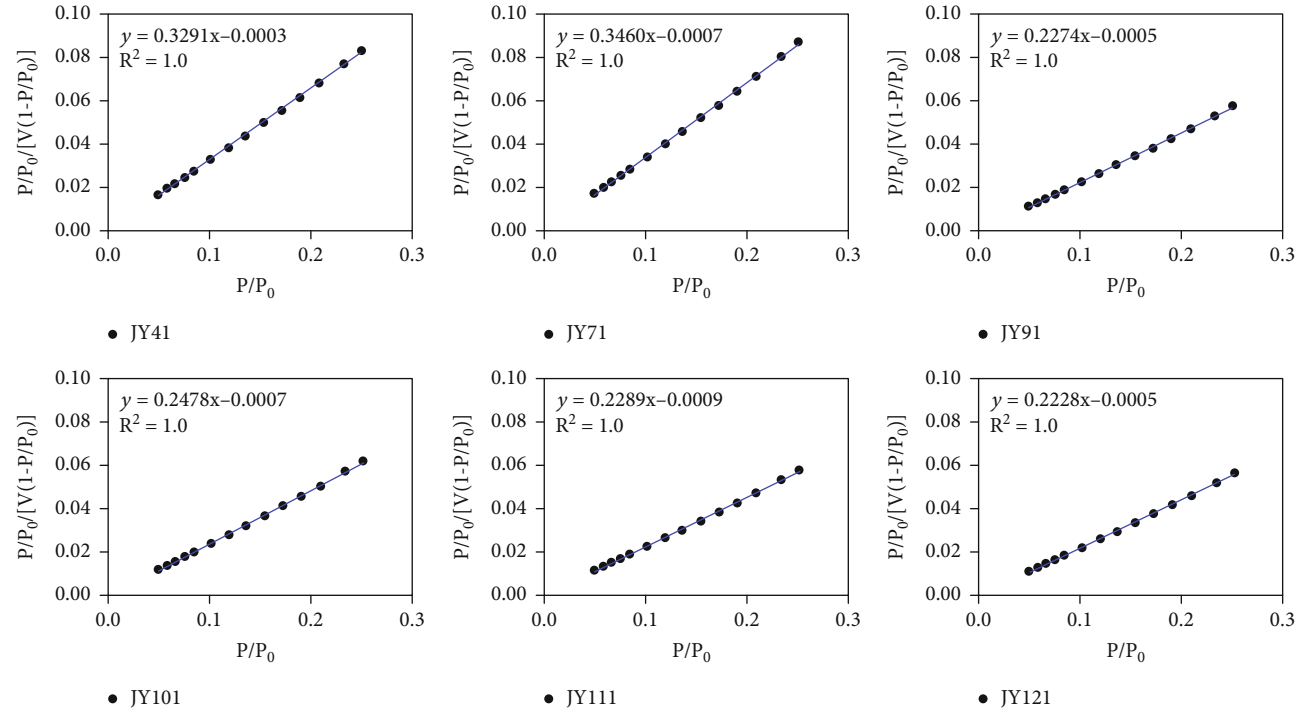

Figure 2: BET plot of the studied gas shales.

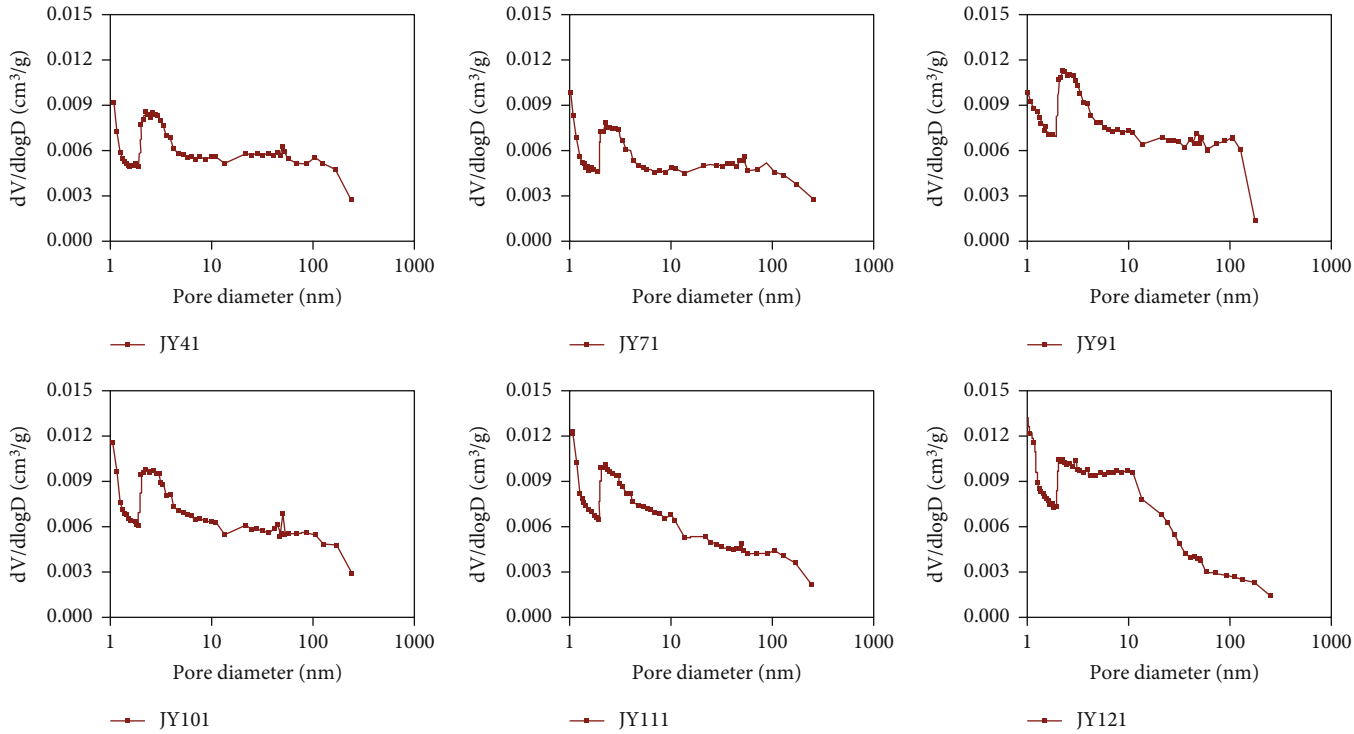

Figure 3: Pore size distribution of shales derived from low-pressure nitrogen adsorption using BJH method.

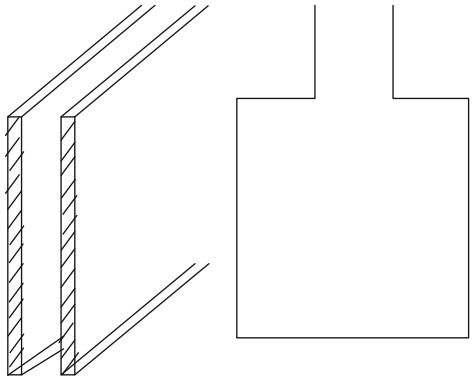

(a) Slit pore (b) Ink-bottle-like pore

Figure 4: Main simplified pore structure in gas shales.

of liquid nitrogen. The critical Kelvin pore radius can be described as

$$r_k = -\frac{2\gamma v_m \cos\phi}{\mathrm{RTln}x}. \quad (3)$$

In the computation of the mesopore size distribution, correction must be made for the effect of the multilayer thickness. The most generally applied thickness emendation methods are those of the Harkin-Jura equation and Halsey equation. In this paper, the Halsey equation is used and can be written as

$$t = -\frac{0.557}{(\log x)^{1/3}}. \quad (4)$$

By the combination of equations (3) and (4), the pore radius of the adsorbent can be calculated as

$$r = r_k + t. \quad (5)$$

As shown in Figure 3, the Jiaoshiba shale samples have wide pore size distributions. Several different peaks appear in the pore size distribution curves, which indicate that these shales have a complicated pore system. The maximum peak values in the pore size distributions range from 2 nm to 4 nm, and the average pore diameter values are mainly concentrated in the 4–10 nm. According to the pore width classification recommended by IUPAC (micropores < 2 nm; mesopores, 2-50 nm; macropores > 50 nm), the average pore diameter of shale samples belongs to mesopores. What is more, a certain amount of

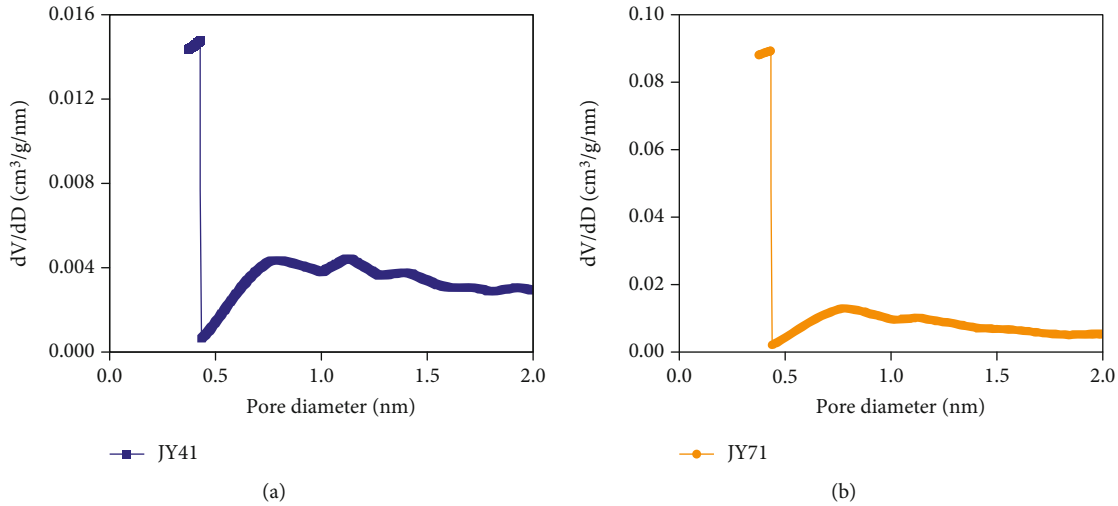

Figure 5: Micropore size distribution of selected gas shales derived from nitrogen adsorption isotherms using the H-K method.

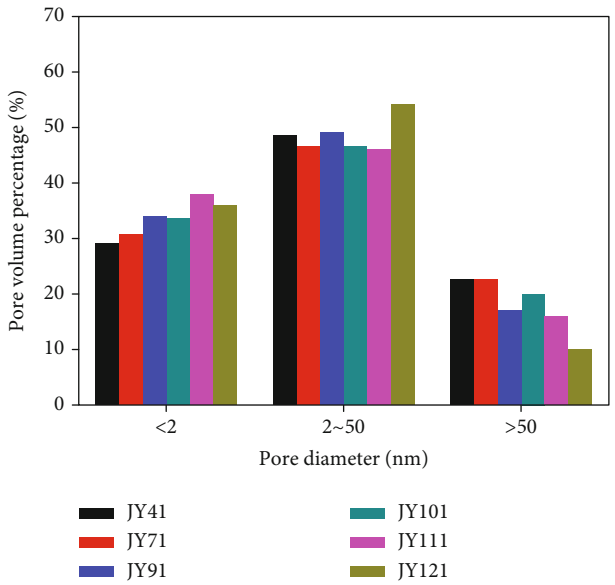

Figure 6: Pore volume percentage of gas shales derived from nitrogen adsorption isotherms.

macropores also exist in shale samples, which cause a tail in the pore size distribution.

Pore structure parameters of the investigated shales are summarized in Table 2. The BET-specific surface area of shales is between 13 and 30 m^2/g. The total pore volume varies from 0.016 to 0.027 cm^3/g. Samples with high TOC content have a higher BET-specific surface area and higher total pore volume, indicating that organic matter is a key control on the pore development of these shales. Specifically, the TOC content of sample JY41 is only 1.0%, and the corresponding BET-specific surface area is 13.9 m^2/g. However, for sample JY121 with a high TOC content of 3.7%, the specific surface area increases to 20.8 m^2/g. The TOC content is positively correlated with the surface area and micropore volume percentage. Meanwhile, the TOC content is negatively correlated with the macropore volume percentage. These results indicate that organic matter mainly affects the development of micropores.

3.4. Adsorption Hysteretic Loop. During the adsorption of mesopores, when the relative pressure of the adsorption system increases to the value corresponding to the Kelvin pore radius, vapors in the pores condense, leading to a steep increase in the adsorption isotherm. When the pressure is lower, the filled pores will be emptied. However, when the curvature of the meniscus of the liquid formed on the adsorption process does not coincide with that on desorption, adsorption hysteresis loops are observed. Thus, the shape of the hysteresis loop gives useful information of the pore structure.

de Boer et al. studied the relationship between the pore structure and the hysteresis loops and summarized five types of hysteresis loops [24]. The IUPAC also recommended an improved classification of hysteresis loops, which consisted of four types. From Figure 1, we can see that the hysteresis loops of the samples exhibit a mixture of type H3 and type H2.

Type H3 is usually found in adsorption isotherms of mesopores with a slit-like shape. As shown in Figure 4(a), meniscus cannot produce before the pressure increase to the saturated vapor pressure of nitrogen in the slit pore, and obvious capillary condensation cannot be observed until the pressure is close to the saturation pressure of nitrogen. After that, the adsorbed films on the parallel plates meet each other, and the pores are full of adsorbate. For the desorption process, evaporation will commence at the relative pressure corresponding to the effective radius of the meniscus until the pore is completely empty, resulting in an abrupt decline in the desorption isotherm.

The hysteretic loop of type H2 is wide, and the desorption isotherm behaves steeply than the adsorption isotherm, which indicates that the pores are ink-bottle-shaped, composed of cylindrical pores closed on the one end and a narrow neck at the other (Figure 4(b)). In these ink-bottle pores,

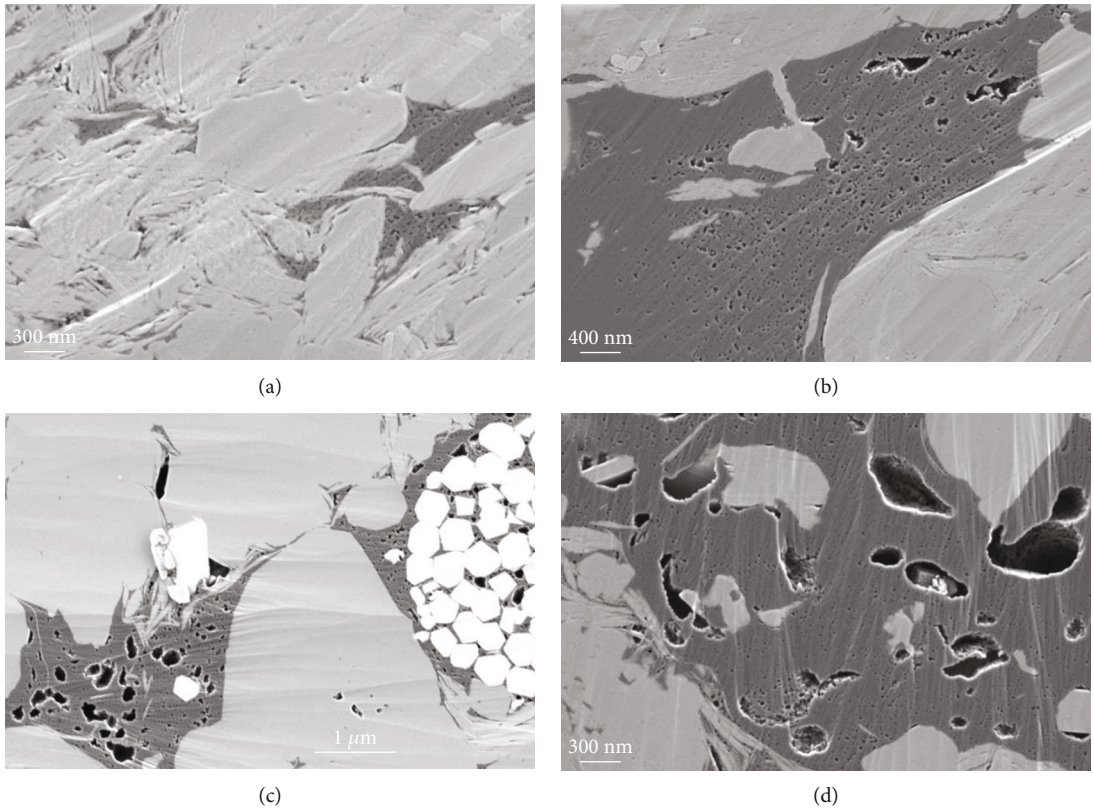

Figure 7: Pore structure of gas shales using FE-SEM technology: (a) sample JY41; (b) sample JY71; (c) sample JY101; (d) sample JY111.

condensation with a hemispherical meniscus occurs at the base and then fills the whole pore because the radius of curvature of the body is less than that of the neck. Evaporation from the full pore will commence in the neck. After that, the pressure is already lower than the value for the body to evaporate, the pore will empty completely, and the desorption branch has a sudden drop in medium pressure.

3.5. Analysis of Micropores. The Horvath-Kawazoe (H-K) model is commonly used to calculate the micropore of shale samples [25]. This model describes the microporous adsorption considering the interaction between the adsorbate and the adsorbent. The H-K model can be expressed as

$$\mathrm{RTln}\frac{P}{P_0} = k\frac{N_a A_a + N_s A_s}{\sigma^4 (L-d)}\left[\frac{\sigma^4}{3(L-d/2)^3} - \frac{\sigma^{10}}{9(L-d/2)^9} - \frac{\sigma^4}{3(d/2)^3} + \frac{\sigma^{10}}{9(d/2)^9}\right]. \quad (6)$$

Figure 5 represents the differential pore volume and pore diameter curve calculated from the H-K model. It can be seen that there are multipeaks in the micropore size distribution curves. The peak values in the micropore size distributions for sample JY41 are 0.45 nm, 0.80 nm, 1.15 nm, and 1.43 nm and that for sample JY71 are 0.43 nm, 0.77 nm, and 1.13 nm. Micropore size distributions of these shales show the trend of decreasing slowly when the pore diameter is above 1.5 nm.

Figure 6 illustrates the ratio of the pore volume of micropores, mesopores, and macropores to the total pore volume. The average ratio of the micropore volume to the total pore volume is around 34%, while the mesopore volume occupies about 48% of the total pore volume. The ratio of the macropore volume to the total pore volume averages 18%. This indicates that the micropores and mesopores are well developed in gas shales and play an important role in the hydrocarbon gas adsorption of shales.

3.6. The Morphology of Pores in Gas Shales. Figure 7 shows FE-SEM images of selected shale samples. Sample JY41 has a relatively high content of clay minerals (53%) and low TOC content (1%), while sample JY101 and JY 111 have a high TOC content (2.2% and 3.3%, respectively). Correspondingly, sample JY41 has a lot of slit-like pores related to clay minerals, while pores in sample JY101 and JY 111 have dominantly organic matter-related pores with an elliptical cross-section, indicating that there are ink-bottle pores inside. With the increase of TOC content, more and more organic matter-hosted pores are developed. Pore size in these shales varies from several to hundreds of nanometers.

4. Discussion

4.1. Geological Controls on Pore Structure of Shales. The pore structure of gas shales is the basis for reservoir evaluation and fluid production prediction. The pore structure of

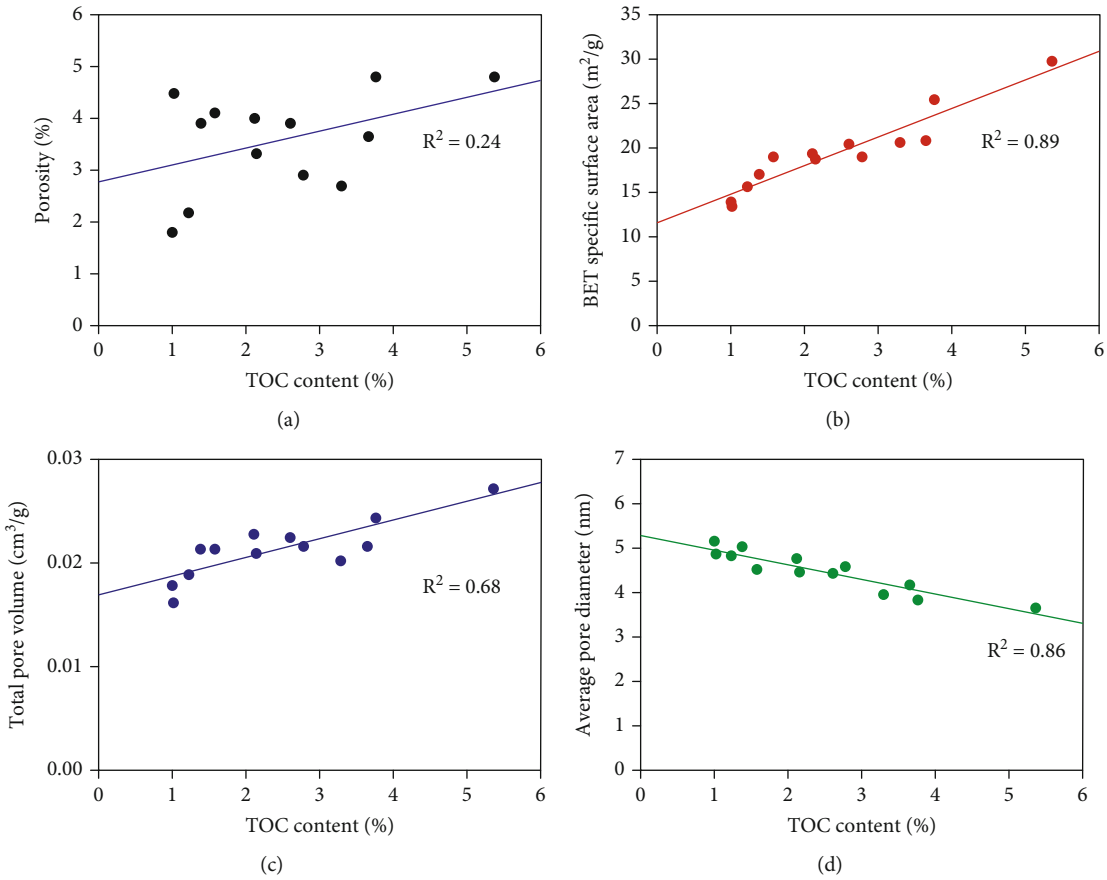

Figure 8: The relationship between TOC content and (a) porosity, (b) BET-specific surface area, (c) total pore volume, and (d) average pore diameter of the studied gas shales using FE-SEM technology.

marine shales from the Sichuan Basin is affected by the organic matter and inorganic matter minerals. As illustrated in Figure 8, a moderate positive relationship exists between the TOC content and the porosity of these shales. This shows that the porosity of marine shales from this area is controlled by organic matter. Organic matter mainly affects the small pores of these investigated gas shales. There is a positive relationship between TOC content and BET-specific surface area and total pore volume. With the TOC content increasing from 1.0% to 5.4%, the specific surface area of the studied shales increases from 14 m^2/g to 30 m^2/g. What is more, an excellent negative relationship exists between the TOC content and the average pore diameter (Figure 8(d)). These all emphasize the role of organic matter on small pores. In the FE-SEM images, there are abundant nanoscaled pores in organic matter particles (Figure 7).

The total pore volume is further divided into the micropore volume, mesopore volume, and macropore volume to analyze the controls on the development of different scale pores. TOC content shows an excellent positive relationship with the micropore volume percentage and a negative relationship with the macropore volume percentage (Figure 9). This further underlines the effect of organic matter on the development of small pores. On the contrary, the total clay mineral content shows negative correlation with the micropore volume percentage. What is more, the macropore volume percentage first increases with the increase of the clay minerals and then decreases again. The macropore volume percentage reaches a maximum when the clay minerals increase to about 45%. These are probably related to the flexibility of clay minerals. With the increase of clay minerals, the macropores develop. However, this increase in ductile clay minerals leads to the decrease in the relative content of rigid minerals (such as quart and carbonates). The ductile clay minerals have difficulty in resisting the compaction of overlying formations; thus, excessive content of clay minerals will decrease the development of macropores.

4.2. Quantitative Contribution of Minerals to Total Porosity. As stated above, the pore structure of shales is controlled by many geological factors. Many investigators have reported the main control of organic matter on pores of highly matured and overmature marine shales. However, not only organic matter but also clay minerals affect the porosity of gas shales. Many interparticle pores even microfractures are formed between the clay minerals and framework minerals. Thus, in order to semiquantitatively estimate the contribution of organic matter and inorganic matter on the pore structure of these gas shales, a simple combined physical model is introduced to calculate the porosity of shales [11,

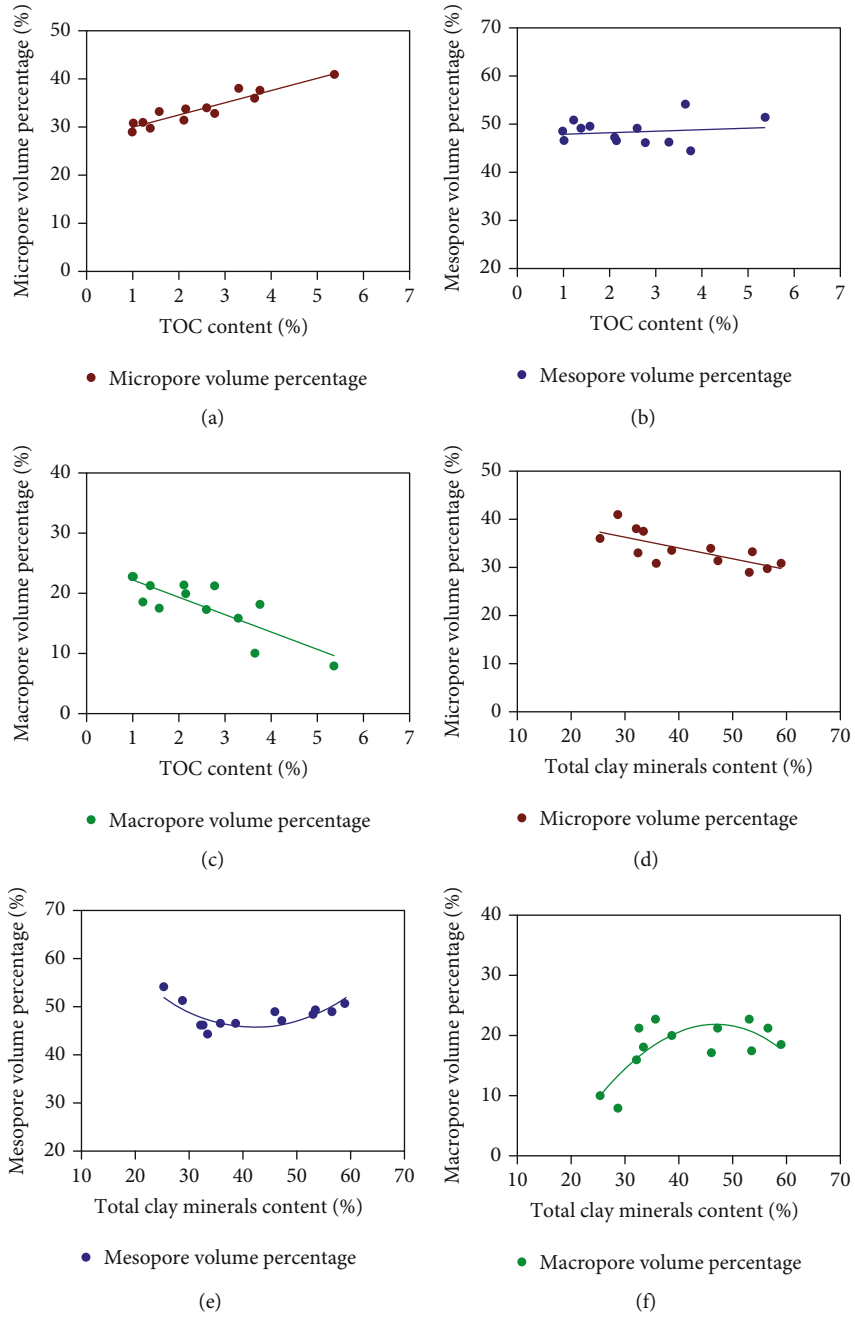

FIGURE 9: The relationship between (a) TOC content and micropore volume percentage, (b) TOC content and mesopore volume percentage, (c) TOC content and macropore volume percentage, (d) clay mineral content and micropore volume percentage, (e) clay mineral content and mesopore volume percentage, and (f) clay mineral content and macropore volume percentage.

26]. Shales are comprised of organic matter, framework minerals (quartz, carbonate, etc.), and clay minerals. The total pore volume of the shale matrix can be approximately viewed as the sum of the pore volume of organic matter (V_{OM}), pore volume of framework minerals ($V_{framework}$), and pore volume of clay minerals (V_{Clay}):

$$V_{pore} = V_{OM} + V_{Framework} + V_{Clay}. \quad (7)$$

Equation (7) can be expanded as

$$V_{pore} = \rho_{bulk} \cdot V_{bulk} \cdot \left[w_{OM} \cdot \bar{v}_{OM} + w_{Framework} \cdot \bar{v}_{Framework} + w_{Clay} \cdot \bar{v}_{Clay}\right]. \quad (8)$$

Here, V_{pore} (cm^3) is the pore volume of the shale; V_{bulk} (cm^3) is the bulk volume and ρ_{bulk} (cm^3/g) is the bulk density; w_{OM}, $w_{Framework}$, and w_{Clay} are the mass fractions of

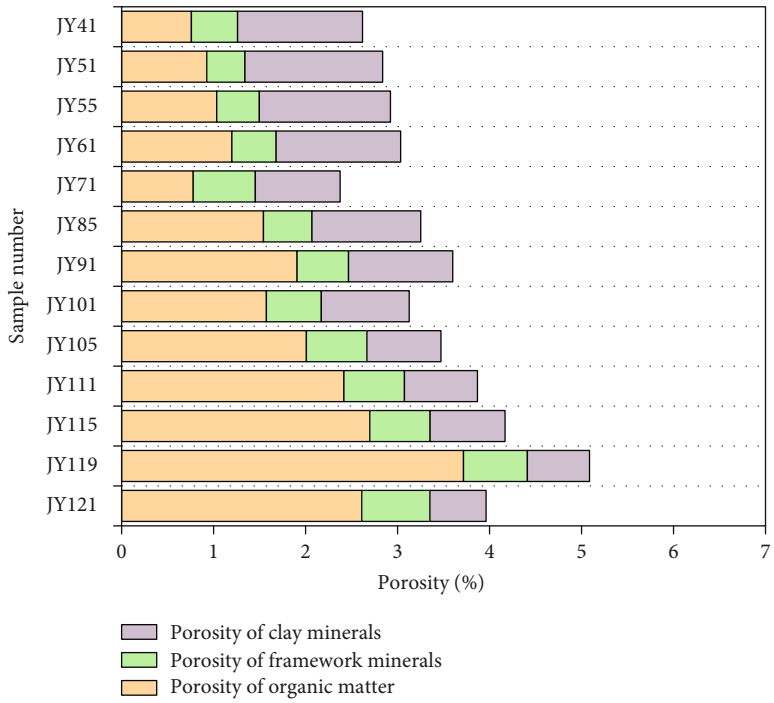

Figure 10: The calculated porosity of organic matter, framework minerals, and clay minerals of the studied shales.

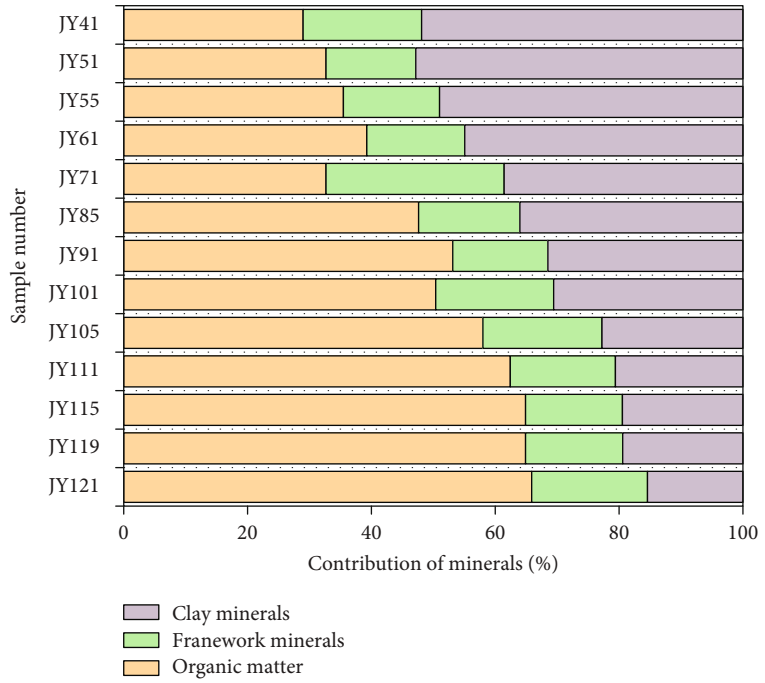

Figure 11: The contribution of organic matter, framework minerals, and clay minerals to the total porosity of the studied shales.

organic matter, framework minerals (quartz, carbonate, et al.), and clay minerals, respectively; and $\bar{v}_{OM}$, $\bar{v}_{Framework}$, and $\bar{v}_{Clay}$ (cm^3/g) are defined as the specific pore volume of organic matter, framework minerals, and clay minerals, respectively.

By introducing the relationship between porosity and pore volume ($\phi = V_{pore}/V_{bulk}$), equation (8) can be further written as

$$\phi = \rho_{bulk} \cdot \left[\frac{w_{TOC}}{0.85} \cdot \bar{v}_{OM} + w_{Framework} \cdot \bar{v}_{Framework} + w_{Clay} \cdot \bar{v}_{Clay}\right]. \tag{9}$$

Combined with the bulk density (ρ_{bulk}) and mass fraction of individual minerals (inorganic matter minerals and organic matter), multielement nonlinear regression was employed to obtain the specific pore volumes of individual minerals ($\bar{v}_{OM}$, $\bar{v}_{Framework}$, and $\bar{v}_{Clay}$). For the investigated gas shales, the fitted $\bar{v}_{OM}$, $\bar{v}_{Framework}$, and $\bar{v}_{Clay}$ are $0.2853\,cm^3/g$, $0.0042\,cm^3/g$, and $0.0096\,cm^3/g$, respectively. The specific pore volume of minerals decreases in the following order: organic matter > clay minerals > framework minerals.

The combined physical model can be employed to semiquantitatively calculate the contribution of major minerals to the total porosity of shales. The helium porosity of the studied gas shales ranges from 1.8% to 4.8%. The contributions of individual minerals to the total porosity can be estimated using the ratio of $\rho_{bulk} \cdot w_i \cdot \bar{v}_i$ to the helium porosity (Figure 10). The calculated contribution of minerals decreases in the following sequence: organic matter (29%–73.1%, average 49.6%) > clay minerals (13.2%–52.8%, average 32.9%) > framework minerals (13.7%–28.9%, average 17.5%) (Figure 11). These results indicate that the total porosity of the investigated shales is controlled by both organic matter and clay minerals, which is consistent with the relations between TOC content and clay minerals and pore structure parameters (Figure 9).

5. Conclusions

The pore structure of shales is analyzed via nitrogen adsorption-desorption isotherms associated with adsorption hysteretic loops. The parameters used for characterizing the pore structure are calculated, including the BET-specific area, pore size distribution, pore volume, and pore diameter. FE-SEM studies are also performed to observe the morphology of the nanopore structure of shales.

(1) The adsorption isotherms of shales belong to the type IV adsorption isotherm, which indicates that the pore structure of shales is complicated and multiscaled, and the pore size ranges from as small as a molecular size about 0.86 nm to being relatively infinite. The adsorption hysteresis loops of Jiaoshiba shales have mixture characteristics mainly of type H3 and type H2. The morphology of the adsorption hysteresis loop demonstrates that the shale samples are mainly parallel slit pores and ink-bottle-like pores

(2) Porosity of the studied shales ranges from 1.8% to 4.8%. The specific surface area of these shales is between 14 and $30\,m^2/g$. There is positive relation between TOC content and the specific surface area. Micropore volume and mesopore volume occupy the total pore volume highly up to 78%–92%, which indicates that micropores and mesopores play an important role in hydrocarbon adsorption and storage

(3) Pore structure of the gas shales studied is mainly related to organic matter and clay minerals. Organic matter is mainly related to the micropores, as shown in the positive relationship between TOC content and micropore volume. Macropores are mainly related to clay minerals. However, if the clay mineral content is too high, it will decrease the pores due to the fact that the ductile clay minerals cannot resist the compaction of overlying formations

(4) The combined physical model offers a fast estimation about the contribution of minerals to porosity of gas shales with similar lithotypes. The results show that organic matter contributes about 50% to the total porosity, while clay minerals contribute about 33% to the porosity of these shales

Nomenclature

P: Equilibrium pressure
P_0: Saturated pressure
S: Specific surface area
V_m: Monolayer capacity
C: BET constant
a_m: Molecular cross-sectional area
K: Avogadro constant, 6.023×10^{23}
r_k: Kelvin radium
γ: Surface tension of condensation liquid
v_m: Volume of condensation liquid
ϕ: Contact angle
x: Relative pressure
t: Adsorption film thickness
R: Universal gas constant
T: Absolute temperature
d_s: Diameter of adsorbent atom, nm
d_a: Diameter of adsorbate atom, nm
σ: Distance between gas and solid atom when their interaction energy is zero
L: Pore diameter
Ns: Number of atom in unit area
As: Kirkwood-Moller coefficient
Aa: Kirkwood-Moller coefficient.

Data Availability

The nitrogen adsorption experiment is conducted on the QUADRASORB SI surface and porosity analyzer, which

uses a static volumetric method to measure the amount of adsorbed gas. This instrument can measure the nanopore ranging from 0.35 nm to 400 nm; the specific surface area detected is 0.0005 m^2/g, and the pore volume is 0.0001 cm^3/g. Before nitrogen adsorption experiments, all the shale samples were degassed at 105°C for more than 8 hours under a vacuum of 10 μm Hg, which ensures removal of any bound and capillary water adsorbed with the clays. Reagent-grade nitrogen (99.999%) is used for adsorbent at 77.35 K. FEI field emission scanning electronic microscopy (FE-SEM) was used to observe the microscope morphology and pore structure. FE-SEM provides "as received" images on a pore structure with high resolution of 1.2 nm and 25-200k magnification, and the tests are preceded on a high vacuum environment. The above experiments were completed at the Research Institute of Exploration and Development, Jianghan Oilfield Branch Company, SINOPEC, and the Key Laboratory of Tectonics and Petroleum Resources (China University of Geosciences), Ministry of Education.

Conflicts of Interest

The authors declare no conflict of interest.

Acknowledgments

The authors would like to acknowledge the financial support of the National Natural Science Foundation of China (No. 41972184).

References

[1] C. R. Clarkson, M. Freeman, L. He et al., "Characterization of tight gas reservoir pore structure using USANS/SANS and gas adsorption analysis," *Fuel*, vol. 95, pp. 371–385, 2012.

[2] C. Lyu, Z. Ning, M. Chen, and Q. Wang, "Experimental study of boundary condition effects on spontaneous imbibition in tight sandstones," *Fuel*, vol. 235, pp. 374–383, 2019.

[3] Y.-b. Lin, J. Zhang, X.-g. Liu, and H.-t. Zhou, "Pore structure features of reservoirs at late high water-cut stage, Lamadian Oilfield, Daqing, China," *Petroleum Exploration and Development*, vol. 35, no. 2, pp. 215–219, 2008.

[4] Y. Shu, S. Xu, F. Yang et al., "The role of microfabric and laminae on pore structure and gas transport pathways of marine shales from Sichuan Basin, China," *Geofluids*, vol. 2020, Article ID 8844229, 19 pages, 2020.

[5] L. Huang, Z. Ning, H. Lin, W. Zhou, and H. Xu, "High-pressure sorption of methane, ethane, and their mixtures on shales from Sichuan Basin, China," *Energy & Fuels*, vol. 35, no. 5, pp. 3989–3999, 2021.

[6] S. Xu, F. Hao, Z. Shu, A. Zhang, and F. Yang, "Pore structures of different types of shales and shale gas exploration of the Ordovician Wufeng and Silurian Longmaxi successions in the eastern Sichuan Basin, South China," *Journal of Asian Earth Sciences*, vol. 193, article 104271, 2020.

[7] R. G. Loucks, R. M. Reed, S. C. Ruppel, and U. Hammes, "Spectrum of pore types and networks in mudrocks and a descriptive classification for matrix–related mudrock pores," *AAPG Bulltin*, vol. 96, no. 6, pp. 1071–1098, 2012.

[8] K. L. Milliken, M. Rudnicki, D. N. Awwiller, and T. W. Zhang, "Organic matter-hosted pore system, Marcellus Formation (Devonian), Pennsylvania," *AAPG Bulltin*, vol. 97, no. 2, pp. 177–200, 2013.

[9] U. Kuila and M. Prassd, "Specific surface area and pore-size distribution in clays and shales," *Geophysical Prospecting*, vol. 61, no. 2, pp. 341–362, 2013.

[10] J. Klaver, G. Desbois, R. Littke, and J. L. Urai, "BIB-SEM characterization of pore space morphology and distribution in postmature to overmature samples from the Haynesville and Bossier shales," *Marine and Petroleum Geology*, vol. 59, pp. 451–466, 2015.

[11] F. Yang, Z. Ning, Q. Wang, R. Zhang, and B. M. Krooss, "Pore structure characteristics of lower Silurian shales in the southern Sichuan Basin, China: insights to pore development and gas storage mechanism," *International Journal of Coal Geology*, vol. 156, pp. 12–24, 2016.

[12] N. S. Fishman, P. C. Hackley, H. A. Lowers et al., "The nature of porosity in organic-rich mudstones of the Upper Jurassic Kimmeridge Clay Formation, North Sea, offshore United Kingdom," *International Journal of Coal Geology*, vol. 103, pp. 32–50, 2012.

[13] F. Yang, B. Lyu, and S. Xu, "Water sorption and transport in shales: an experimental and simulation study," *Water Resources Research*, vol. 57, no. 2, article e2019WR026888, 2021.

[14] M. Gasparik, A. Ghanizadeh, P. Bertier, Y. Gensterblum, S. Bouw, and B. M. Krooss, "High-pressure methane sorption isotherms of black shales from the Netherlands," *Energy & Fuels*, vol. 26, no. 8, pp. 4995–5004, 2012.

[15] F. Yang, H. Zheng, B. Lyu, F. Wang, Q. Guo, and H. Xu, "Experimental investigation about gas transport in tight shales: an improved relationship between gas slippage and petrophysical properties," *Energy & Fuels*, vol. 35, no. 5, pp. 3937–3950, 2021.

[16] F. Yang, B. Hu, S. Xu, Q. Meng, and B. M. Krooss, "Thermodynamic characteristic of methane sorption on shales from oil, gas, and condensate windows," *Energy & Fuels*, vol. 32, no. 10, pp. 10443–10456, 2018.

[17] J. X. Dai, C. N. Zou, S. M. Liao et al., "Geochemistry of the extremely high thermal maturity Longmaxi shale gas, southern Sichuan Basin," *Organic Geochemistry*, vol. 74, pp. 3–12, 2014.

[18] T. L. Guo and H. Zhang, "Formation and enrichment mode of Jiaoshiba shale gas field, Sichuan Basin," *Petroleum Exploration and Development*, vol. 41, no. 1, pp. 31–40, 2014.

[19] T. L. Guo, "Key geological issues and main controls on accumulation and enrichment of Chinese shale gas," *Petroleum Exploration and Development*, vol. 43, no. 3, pp. 349–359, 2016.

[20] IUPAC, "Reporting physisorption data for gas/solid systems with special reference to the determination of surface area and porosity (recommendations 1984)," *Pure and Applied Chemistry*, vol. 57, no. 4, pp. 603–619, 1985.

[21] S. J. Gregg and K. S. W. Sing, *Adsorption, surface area and porosity*, Academic Press, London, 1982.

[22] S. Bruauer, P. H. Emmett, and E. Teller, "Adsorption of gases in multimolecular layers," *Journal of the American Chemical Society*, vol. 60, no. 2, pp. 309–319, 1938.

[23] E. P. Barrett, L. G. Joyner, and P. Halenda, "The determination of pore volume and area distributions in porous substances. I.

Computations from nitrogen isotherms," *Journal of the American Chemical Society*, vol. 73, no. 1, pp. 373–380, 1951.

[24] J. H. de Boer, D. H. Everett, and F. S. Stone, *The Structure and Properties of Porous Materials*, Butterworth Publishing Company, Oxford, 1958.

[25] G. Horvath and K. J. Kawazoe, "Method for the calculation of effective pore size distribution in molecular sieve carbon," *Journal of Chemical Engineering of Japan*, vol. 16, no. 6, pp. 470–475, 1983.

[26] Y. M. Wang, D. Z. Dong, H. Yang et al., "Quantitative characterization of reservoir space in the Lower Silurian Longmaxi Shale, southern Sichuan, China," *Science China Earth Sciences*, vol. 57, no. 2, pp. 313–322, 2014.